# Bulk electronic transport impacts on electron transfer at conducting polymer electrode–electrolyte interfaces

Kosala Wijeratne[a,1], Ujwala Ail[a,1], Robert Brooke[a], Mikhail Vagin[a], Xianjie Liu[b], Mats Fahlman[b], and Xavier Crispin[a,2]

[a]Department of Science and Technology, Linköping University, 60174 Norrköping, Sweden; and [b]Department of Physics, Chemistry, and Biology, Linköping University, 58183 Linköping, Sweden

Edited by John A. Rogers, Northwestern University, Evanston, IL, and approved October 15, 2018 (received for review April 9, 2018)

**Electrochemistry is an old but still flourishing field of research due to the importance of the efficiency and kinetics of electrochemical reactions in industrial processes and (bio-)electrochemical devices. The heterogeneous electron transfer from an electrode to a reactant in the solution has been well studied for metal, semiconductor, metal oxide, and carbon electrodes. For those electrode materials, there is little correlation between the electronic transport within the electrode material and the electron transfer occurring at the interface between the electrode and the solution. Here, we investigate the heterogeneous electron transfer between a conducting polymer electrode and a redox couple in an electrolyte. As a benchmark system, we use poly(3,4-ethylenedioxythiophene) (PEDOT) and the Ferro/ferricyanide redox couple in an aqueous electrolyte. We discovered a strong correlation between the electronic transport within the PEDOT electrode and the rate of electron transfer to the organometallic molecules in solution. We attribute this to a percolation-based charge transport within the polymer electrode directly involved in the electron transfer. We show the impact of this finding by optimizing an electrochemical thermogalvanic cell that transforms a heat flux into electrical power. The power generated by the cell increased by four orders of magnitude on changing the morphology and conductivity of the polymer electrode. As all conducting polymers are recognized to have percolation transport, we believe that this is a general phenomenon for this family of conductors.**

conducting polymer | electron transfer | thermogalvanic cell

Heterogeneous electron transfer (HET) takes place at the interface between a solid electrode and a reactant in a liquid electrolyte. HET is of uttermost importance in many technologies today, such as corrosion protection, fuel cells, batteries, medical sensors, organic electrochemical synthesis, food analysis, and electronics. The rate of the HET depends on the type of reactants, electrodes, solvents, and electrolyte. Interestingly, HET has been studied on various types of planar and nonporous electrodes: liquid and solid metals, semimetals such as graphite, and inorganic semiconductors. HET can be classified in two routes: when the reactant can (cannot) chemisorb on the electrode; in that case, the HET is called "inner sphere" and fast ("outer sphere" and slow), indicating strong (weak) electronic coupling between the electrode and the reactant (1). In first approximation (2), the faradic current $i_f$ generated by the HET is proportional to the kinetic constant of the reaction $k_o$, the density of surface charge carriers of relevant energy $N_s(E)$, the concentration of reactant at the surface $C^R{}_s$, and an energy distribution function related to the electronic level of the reactant-involved $W^R(E)$:

$$i_f = k_o N_s(E) C_s^R W^R(E). \quad [1]$$

An electron transfer at semiconductor or semimetal electrodes is often slower than that on metals, not necessarily because of the absence of chemisorption but rather, because of a low density of electronic states $N(E)$ and a corresponding low density of charge carriers (3). The faradic current from the HET can also be enhanced with porous electrodes of the large surface area (4) with the extreme case of carbon nanotubes. Metallic carbon nanotubes have a surface area of 1,100 $m^2/g$ (5). For a wide range of potential, the nanotubes are stable and metallic, thus constituting a good electrode. Finally, there exist conducting polymer electrodes that resemble none of the existing classes of materials. However, they have unique features, making them attractive for electrocatalysis (6), fuel cells (7), batteries (8), and sensors (9).

Conducting polymers have a lower density of state typically at the Fermi level than metals, which is also reflected by their modest conduction (1–4 × $10^3$ S/cm), approaching that of bad metals, like Hg ($10^4$ S/cm), but much less conducting than Cu (6 × $10^5$ S/cm). Compared with the metal electrode, we can distinguish four major unique features. First, conducting polymers are stable in air and do not form an insulating oxide layer like conventional nonnoble metals. Second, when swelled in a solvent, they possess a molecular porosity, enabling some small molecular reactants to penetrate the bulk of the electrode: thus, potentially, an intrinsic very high surface area for small reactants. Third, the presence of noncovalent bonds between the polymer chains makes them favorable for ion transport. Hence, conducting polymers are classified among the mixed electron–ion conductors (10). Fourth, they are electrochemically active solids (11, 12). Hence, the electron transfer with the reactant in the

## Significance

**Spreading electrochemical technologies, such as energy, bio-electrochemical devices, and industrial electrochemical synthesis, require low-cost large area electrodes. Conducting polymers possess a unique combination of properties compared with most of the inorganic electrodes: acid resistance, the absence of surface-insulating oxide, low temperature and solution processability, a high natural abundance of their elements, molecular porosity. Conducting polymers are inhomogeneous conductors composed of ordered and disordered regions through which electronic transport takes place via percolation paths. We discovered that the density of percolation paths in the bulk of the material dictates the rate of electron transfer at the electrolyte–polymer electrode interface. This reveals one of the key parameters of designs to achieve efficient electrochemical technologies based on polymer electrodes.**

Author contributions: K.W. and X.C. designed research; K.W., U.A., R.B., X.L., and M.F. performed research; K.W. contributed new reagents/analytic tools; K.W., U.A., M.V., X.L., and M.F. analyzed data; and K.W. and X.C. wrote the paper.

The authors declare no conflict of interest.

This article is a PNAS Direct Submission.



[1]K.W. and U.A. contributed equally to this work.

[2]To whom correspondence should be addressed. Email: xavier.crispin@liu.se.

This article contains supporting information online at www.pnas.org/lookup/suppl/doi:10.1073/pnas.1806087115/-/DCSupplemental.

Published online November 5, 2018.

solution must occur at an electrochemical potential corresponding to the conducting state of the polymer electrode; otherwise, the polymer would be insulating and cannot play the role of an electrode (i.e., no efficient electron transfer can occur) (8). A recent study shows the irreversible and strong potential dependence of the rate of electron transfer on the density of state of the polymer electrode in that specific case where the energy distribution function $W^R(E)$ of the reactant is located at the band edge of the polymer electrode [that is, where the $N_s(E)$ drops to zero in the band gap (13)]. Finally, the chemical structure of the polymer electrode creates specific catalytic sites boosting electrocatalytic reactions, such as, for example, $CO_2$ reduction (14) and $O_2$ reduction (15). This is an exciting avenue, because the chemical design of the polymer can be optimized for a specific electrochemical reaction.

Although semimetallic (16) and metallic behaviors (17, 18) have been found in specific samples in conducting polymers with conductivity decreasing on heating, paracrystalline or amorphous doped polymers usually display a temperature-activated transport in a large temperature range (19). Conducting polymers appear as inhomogeneous solid in which the transport is limited by the connectivity of conducting ordered domains because of the presence of poorly conducting disordered domains acting as an energy barrier; the latter causes the temperature dependency of conductivity. In these materials, percolation transport is proposed as a predominant mechanism (20, 21). Poly(3,4-ethylenedioxythiophene) (PEDOT) complexed with polystrenesulfonic acid is used as a benchmark system, because it is the most widely used among all intrinsically conducting polymers due to its water processability, its high electrical conductivity (up to about 1,000 S/cm), and good air stability (22). The chemical structures are presented in Fig. 1. The sulfonate-to-thiophene ratio is about three, indicating a clear excess in polystryrenesulfonate (PSS) not involved in the neutralization of the positively charged PEDOT chains (23). The PEDOT-PSS nanoparticles are 20–30 nm in diameter in solution (24). They possess a PEDOT-PSS core and a negatively charged PSS shell to promote repulsion of the nanoparticles and stabilize the suspension. The water evaporation leads to a morphology clearly coming from the composition of the nanoparticles (25), where the excess of PSS insulating shell acts as a barrier for the charge transport. While PEDOT-PSS typically has a modest conductivity of about 1 S/cm, it can be enhanced by three orders of magnitude through a change of morphology (i.e., without varying its oxidation level) (26). This is realized by adding a so-called secondary dopant, which is a high boiling point solvent, such as DMSO, that phase separates the excess PSS into nanodomains to create percolation paths of highly conducting PEDOT-PSS (27, 28). Hence, one more difference with metals is that the conductivity of polymers strongly depends on the microscopic morphology and self-organization of the polymer chains. The presence of a metallic character in some temperature range (29) suggests that conducting polymers should be described by a heterogeneous model with small nanocrystallites of aligned chains surrounded by regions where the chains are disordered. While the electronic transport of those materials has been studied abundantly (29, 30), no studies, however, are available to correlate the electrical properties of the polymer electrode with the HET to a reactant in an electrolyte.

In this work, we study the HET between the PEDOT-PSS and a Ferro/ferricyanide redox couple in aqueous electrolyte (Fig. 1). We investigate the interplay between the electrical conductivity of the polymer, its density of state $N_s(E)$, and the rate of electron transfer $k_o$ to the reactant and show that an additional phenomenon is involved in the description of HET at conducting polymer electrodes. We use this knowledge to optimize the electrical power generated by a thermogalvanic cell (TGC), which is an electrochemical device that converts a heat flow into electricity.

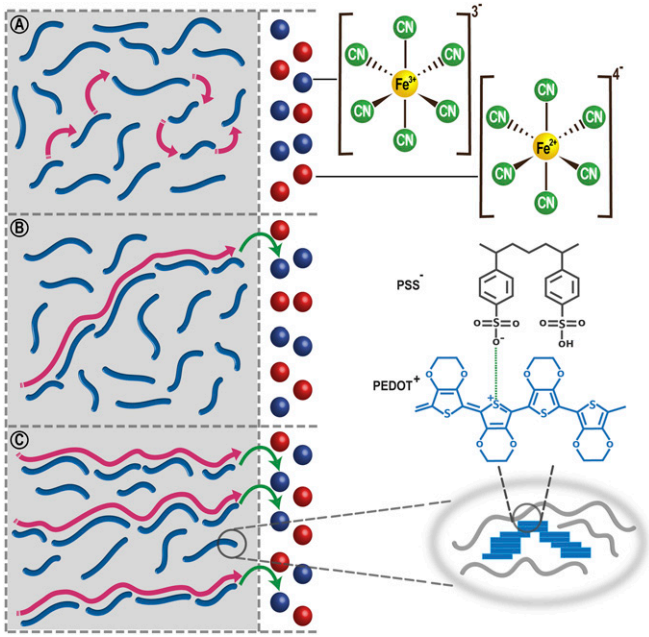


**Fig. 1.** Schematic diagram of charge transport (pink arrows) within the polymer electrode and the electron transfer (green arrows) at the polymer electrolyte interface for (*A*) poor-conducting, (*B*) intermediate-conducting, and (*C*) high-conducting PEDOT-PSS electrodes. The blue "snake" lines (on left-hand side) mimic aggregates of PEDOT chains that display short-range order through π–π stacks.

## Results and Discussion

Importantly, we do not use a metallic electrode underneath the polymer electrode to avoid any parasitic side reaction with the metal and to truly reveal the interplay between HET and electronic transport within the polymer. Our choice of PEDOT-PSS and Ferro/ferricyanide redox electrolyte provides an ideal model system for this type of study for the following reasons. First, the electrical conductivity of PEDOT-PSS can be tuned over three orders of magnitude simply by adding DMSO in the water suspension through a morphology change well known in the literature. Hence, this so-called secondary doping effect provides a key feature to investigate the impact of the bulk transport on the HET at conducting polymer electrolyte–electrolyte interface. Second, both forms of the redox couple Ferro/ferricyanide are negatively charged, and this prevents the reactant from penetrating deep into the PEDOT-PSS electrode, since PSS is the dominant component and acts as anion exclusive membrane. Third, there is likely no chemisorption and no strong electronic coupling between PEDOT and the iron atom in the center of Ferro/ferricyanide. Indeed, six cyanide ligands surround the iron atom, thus ensuring a heterogeneous outer-sphere electron transfer (1). Note that, with metals or inorganic semiconductors, dangling bonds or 3d orbitals favor the chemisorption of the cyanide groups and the destabilization of the organometallic complex, which is not the case for polymer electrodes.

The secondary doping effect of PEDOT-PSS on the addition of DMSO is a well-studied phenomenon in the literature (27, 28). The difference between those studies and our study is that we introduce a cross-linking agent [3-glycidoxypropyltrimethoxysilane (GOPS)] to stabilize PEDOT-PSS films in aqueous media (31). We here show that the addition of GOPS does not affect the secondary doping phenomenon. PEDOT-PSS thin films (220 ± 10 nm) are fabricated by spin coating a commercial PEDOT-PSS water dispersion (PH1000; 1.3 wt % of PEDOT-PSS) on Si substrates (p type, 1,000-nm thermal oxide layer). PH1000 is modified with

various amounts of DMSO up to 6 wt %. The electrical conductivity measured with a four-point probe technique is reported as a function of DMSO content. A sigmoid evolution is observed starting with low conductivity (0.4 S/cm) for pristine PEDOT-PSS (0 wt % DMSO) to 805 S/cm for 5% DMSO (Fig. 2*A*). Our maximum conductivity (805 S/cm) is slightly lower than in previous reports (890 S/cm) (32). The high conductivity obtained for the best PEDOT-PSS morphology is explained by a high-oxidization/doping level [on average, one positive charge for three monomer units (23)] in combination with high mobility of about 0.3–2.7 $cm^2\ V^{-1}\ s^{-1}$ (10, 19). The surprising high mobility observed while PEDOT-PSS is rather amorphous indicates that the charge transport is governed by short-range order (33, 34) into small nanocrystalline domains, as also evidenced by the presence of π–π stacking (35) in the overall amorphous solid. The sigmoid behavior is in agreement with previous observation of a phase separation phenomenon within the PEDOT-PSS blend associated with a separation of the excess PSS (26). The amount of PEDOT metallic nanocrystals is not dramatically changed with the DMSO content as indicated by two observations. First, the absorption spectrum is practically unchanged with a large absorption background in the infrared specific to Drude-like absorption features typical of metallic domains (36) (*SI Appendix*, Fig. S1). Second, the surface density of state $N_s(E)$ at the Fermi level measured by UV-photoelectron spectroscopy (UPS), which indicates a vanishingly small band gap, does not change despite the variation in DMSO content (Fig. 2*B*). While UPS is performed in vacuum, we also confirm that the electrochemical potential of the PEDOT-PSS electrode does not change with the DMSO content when it is swelled with an aqueous electrolyte (*SI Appendix*, Fig. S2). Hence, the three-orders of magnitude increase in conductivity is attributed to the formation of percolation paths realized by a reorganization of the morphology at the nanoscale to promote better connectivity between the metallic-like nanocrystals (10, 20, 21). The model proposed in the literature is in agreement with what is found here despite the addition of GOPS. Fig. 1 shows the formation of percolation paths within the PEDOT electrode. The better conductivity is indicated by a lowering of the activation energy for the transport extracted from a simple Arrhenius law of the conductivity vs. temperature close to room temperature (Fig. 2*C*). Detailed explanation of the activation energy calculation is available in *SI Appendix*, *Note 1* and Fig. S3. Hence, the effect of DMSO is to improve the conductivity of a constant number of metallic-like nanocrystals (local order between PEDOT chains) but without delocalizing the electronic wave function of the nanocrystals over the solid. Hence, the electrical transport occurs through percolation paths characterized by a temperature-activated hopping or ultimately, tunneling at high DMSO content (29).

We now turn to the characterization of the HET. For thick (2,000-nm) PEDOT-PSS film with 5% DMSO (dashed line in *SI Appendix*, Fig. S4), the cyclic voltammogram is composed of a capacitive current (square box $i_c$) and a faradic current (peak $i_f$) contribution. The capacitive contribution is proportional to the film thickness, indicating that small ions penetrate through the film, whereas the faradic contribution is constant, with the film thickness suggesting that the redox molecules do not penetrate in the PEDOT-PSS films (*SI Appendix*, Fig. S5). For thin films of low DMSO content, no visible faradic process takes place despite the presence of Ferro/ferricyanide in the electrolyte due to the low conductivity of the PEDOT-PSS electrode (Fig. 3*A* and *SI Appendix*, Fig. S6). The increase of the DMSO content leads to the appearance of faradic peak currents. The clear transition from slow quasireversible to fast reversible electrode process is indicated by both an increase of peak current and a decrease of the potential of peak-to-peak separation. It is, however, difficult to draw more conclusions based on this dynamic technique due to the complexity of the phenomena and that the electroactivity of the electrode itself depends on its conductivity (*SI Appendix*, Figs. S7 and S8). To decouple the effect of the capacitive charging of the electrode and the HET kinetics, we measure the faradic current in steady state (Fig. 3*B*). As mentioned above, since the density of state does not depend on the DMSO content,

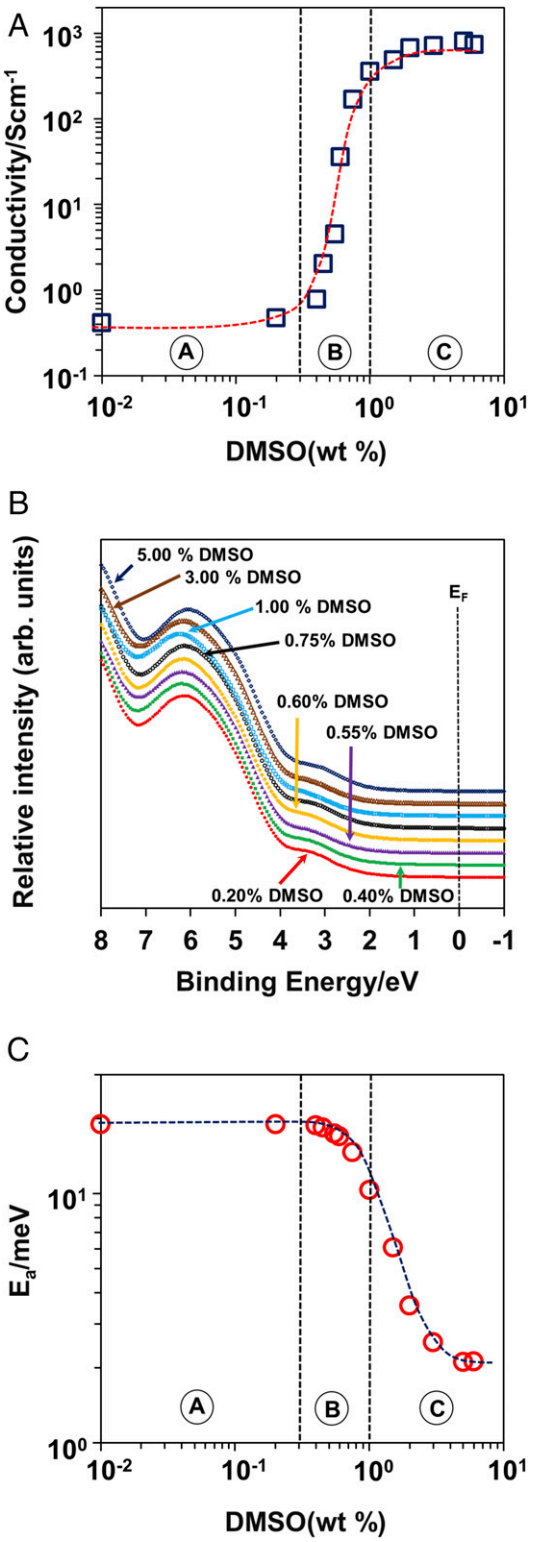


**Fig. 2.** (*A*) Conductivity of PEDOT-PSS-DMSO electrodes. (The dashed red line demonstrated the trend in the electrical conductivity with respect to the DMSO weight %.) (*B*) UPS of PEDOT-PSS-DMSO electrodes. (*C*) Activation energy of PEDOT-PSS-DMSO electrodes. The dashed lines in *A* and *C* are guides for the eyes to follow the trends.

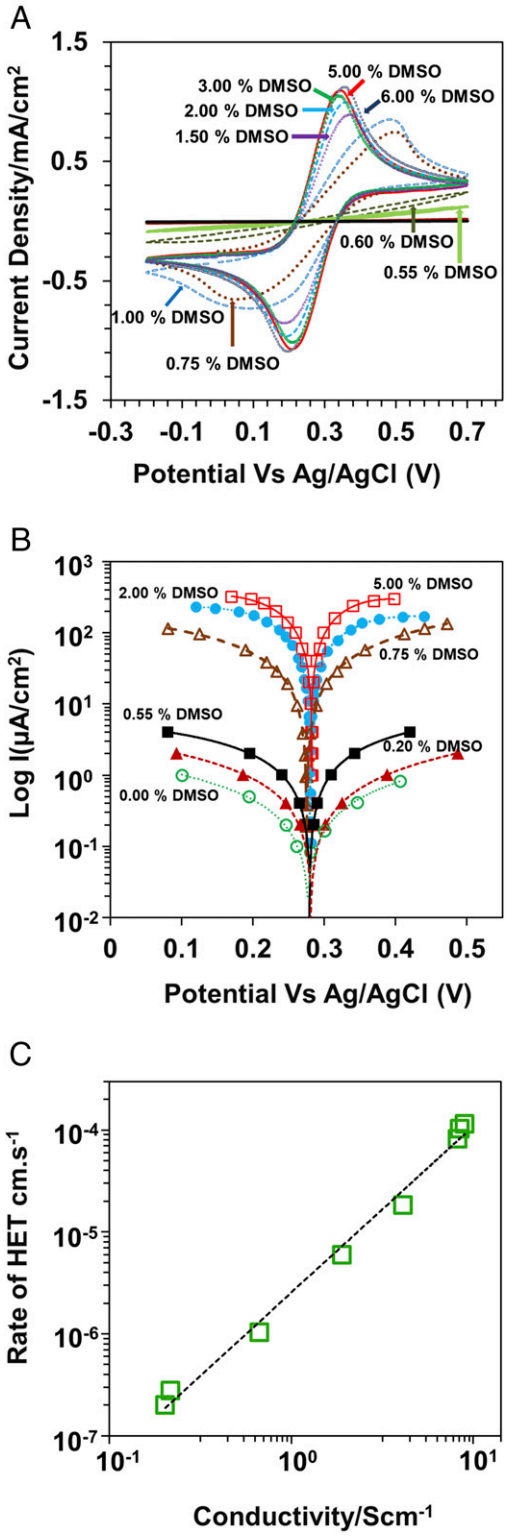


**Fig. 3.** Cyclic voltammetry results of $K_3Fe(CN)_6/K_4Fe(CN)_6$ in KCl solution. (*A*) For different DMSO ratios of PEDOT-PSS-DMSO electrodes, the scan rate is 10 mV $s^{-1}$ (current normalized with the geometric surface area). (*B*) Tafel plot of PEDOT-PSS-DMSO. (*C*) Rate constant of HET vs. the conductivity of PEDOT-PSS electrodes. (The dashed line demonstrated the trend in the exchange current density with respect to the conductivity.)

we believe that the reading of the faradic current will be directly related to the rate constant of the redox process. The steady-state measurements on films of both high and low conductivities enable the quantification of electrode kinetics through the exchange current (*SI Appendix*, *Note 2*, Fig. S9, and Table S1).

We extract the overall rate constant $k_o$ of the HET and compare with the literature: the $k_o$ value obtained for the pristine PEDOT-PSS electrode (low conductivity) is five orders of magnitude lower compared with a flat platinum electrode for Ferro/ferricyanide redox couple in aqueous electrolyte (37, 38). However, an increase of DMSO content leads to an increase in the rate constant, and a three-orders of magnitude increase is observed for the PEDOT-PSS electrode with the highest content of DMSO. For inorganic electrodes, there is no obvious correlation between the charge transport within the bulk of the electrode and the rate of HET taking place at the electrode–electrolyte interface; here, we observe a clear linear correlation between the log $k_o$ and the logarithm of the electrical conductivity of the polymer electrode (Fig. 3*C* and *SI Appendix*, Table S1). Our results show that the overall rate of HET $k_o$ depends on the number of percolations paths, $P_s$, available for the electronic transport within the polymer electrode that reaches the interface between the electrode surface in contact with the electrolyte. Hence, the local rate of electron transfer at the active surface site connected to the percolation path is $k_{ET}$, and the overall rate is $k_o = k_{ET}P_s$. This phenomenon is pictured in Fig. 1, showing how percolation paths lead to HET at the polymer–electrolyte interface. That an interfacial HET is governed by the bulk properties of an electrode has never been seen in any other materials than conducting polymers, and we thus can add one more parameter and express the faradic current as

$$i_f = k_{ET}N_s(E)P_sC_s^RW^R(E). \quad [2]$$

We now apply our findings to TGCs. A TGC (Fig. 4*A*) is an electrochemical power source that consists of two electrodes in contact with the redox electrolyte solution. The TGC differs from conventional semiconductor-based thermoelectric generator devices (39), because the key phenomenon generating voltage involves an electron transfer between an electrode and a redox mediator in an electrolyte. The open circuit thermovoltage ($V_{oc}$) generated by the application of a temperature difference ($\Delta T$) across the TGC can be evaluated by the Seebeck coefficient $S_e = V_{oc}/\Delta T$ (40, 41), and the entropy change in a redox electrolyte equilibrium is the main origin of the thermovoltage (42, 43). The Ferro/ferricyanide redox couple has been widely studied for TGCs due to its good solubility in water and high exchange currents on metal electrodes, yielding a high Seebeck coefficient (1.4 mV/K) (39, 43–47). In our device, both electrodes are based on PEDOT-PSS without metal underneath. In those electrochemical devices, the electrolyte composition is constant 0.4 M $K_4Fe(CN)_6/K_3Fe(CN)_6$, and only one parameter is varied: the conductivity of the two PEDOT-PSS electrodes.

Before applying a temperature gradient, we first study the electrochemical phenomena at one PEDOT-PSS electrode in the isothermal condition by impedance spectroscopy. In other words, we replace one of the PEDOT-PSS electrodes with a Pt mesh and characterize on the remaining polymer electrode. The equivalent circuit used to extract the physical parameters has been proposed by others for similar systems (46, 48) (*SI Appendix*, Figs. S10 and S11 and Table S2). The components are the following: electron transfer resistance ($R_{ET}$), Ohmic serial resistance (electrolyte and interfacial contact resistances; $R_S$), and bulk electrode resistance ($R_F$). Note that $R_F$ values are similar to the measured dc resistance of the polymer film for all values of DMSO content, thus supporting the physical meaning of the circuit component (*SI Appendix*, Fig. S12). For all DMSO

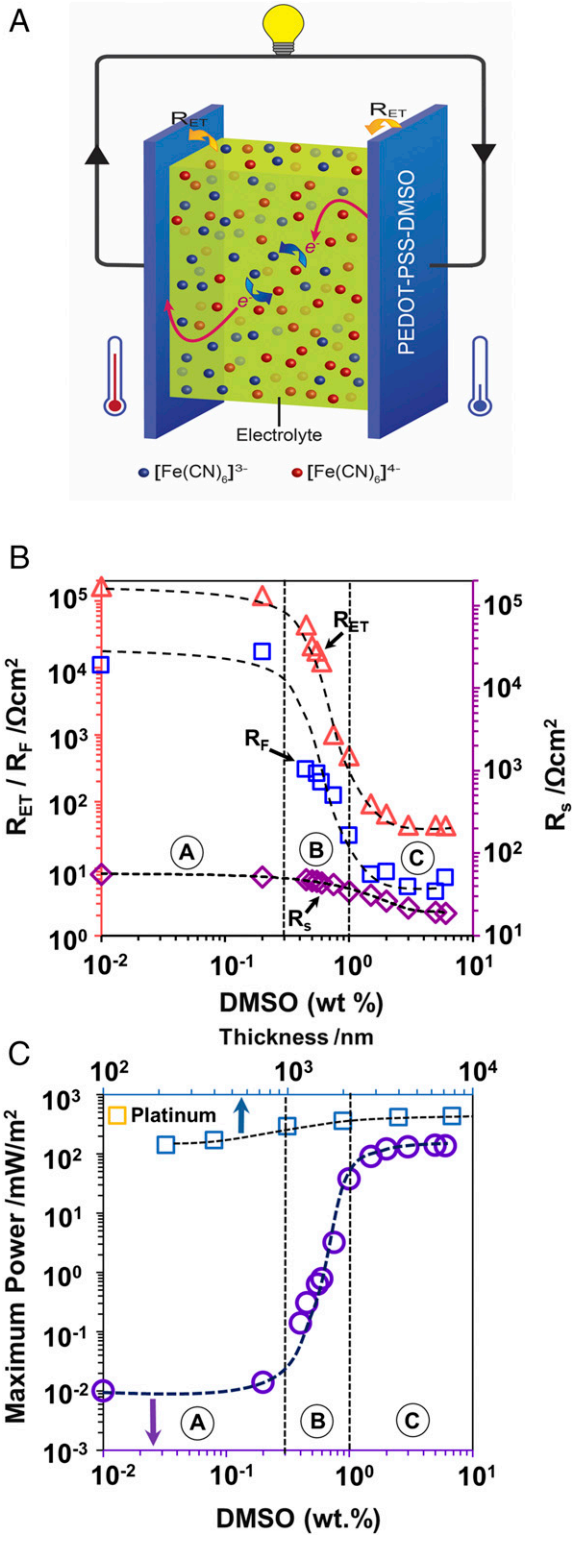


**Fig. 4.** (*A*) Schematic diagram of TGC. (*B*) Charge transfer resistance ($R_{CT}$), Ohmic resistance ($R_S$), and bulk electrode resistance ($R_F$) of PEDOT-PSS-DMSO electrodes. (*C*) Maximum power out of TGC as a function of DMSO ratio and maximum power out of TGC as a function of different thicknesses of PEDOT-PSS-5% DMSO. The dashed black lines are guides for the eyes to show the trend in those graphs. All measurements are taken with a temperature gradient of 30 °C.

contents, $R_{ET}$ is dominant compared with $R_F$ and $R_S$ (Fig. 4*B*). In other words, the electron transfer process is decoupled from the charge transport process in the polymer electrode in all samples, because its kinetics is slower, and it will limit the measured current. Interestingly, the shape of the evolution of $R_{ET}$ vs. DMSO follows a parallel evolution to $R_F$, indicating that the two different phenomena are correlated. This fully supports the independent observation that the rate of electron transfer is related to the conductivity of the films (Fig. 3*C*). $R_{ET}$ dramatically changes from 100,000 to 100 Ωcm$^2$. The kinetics of the dynamic equilibrium for the electron transfer established at the electrode–electrolyte interface is expected to control the TGC performance.

Under temperature gradient between the two PEDOT-PSS electrodes, a thermovoltage is developed, and Seebeck coefficients of 1.43–1.46 mV/K for all PEDOT-PSS blends are extracted, which is in a good agreement with previously reported values with other metal electrodes (39, 49, 50). The independence of the Seebeck coefficient with the DMSO content illustrates the thermodynamic control in the thermovoltage measurements. A dynamic equilibrium of the Ferro/ferricyanide redox process is established even for films of poor conductivity. In contrast, a significant effect of the secondary dopant DMSO content is observed on the power generated by the TGCs acquired at a temperature difference $\Delta T$ = 30 °C (Fig. 4*C* and *SI Appendix*, Fig. S13). The power increases from 0.01 to 140 mW/m$^2$ on DMSO increase, which indicates that the efficiency of the thermogenerator is limited by the electron transfer kinetics. Hence, the four-orders of magnitude increase in both the maximum power density of the TGC and the electrical conductivity of the electrodes (Fig. 2*A*) is correlated to the electron transfer resistance in the impedance data (Fig. 4*B*) and the exchange current in the Tafel plot (Fig. 3*C*). The maximum power can be further enhanced by increasing the thickness of the PEDOT-PPS electrode (from a dispersion with 5 wt % DMSO) from 220 to 4,000 nm to reach 410 mW/m$^2$, which is like the maximum power obtained with platinum electrodes (435 mW/m$^2$). Note, however, that this increase of power is not due to the penetration of the redox molecule in the film (*SI Appendix*, Fig. S5) but due to the transition to another limiting mechanism. Indeed, for thin film electrodes (thickness = 220 nm), the limiting phenomenon is the charge transfer resistance, while for thicker films, $R_S$ becomes limiting (*SI Appendix*, Fig. S14) as found for PEDOT-Tos [poly(3,4-ethylenedioxythiophene)-tosylate] (51). Hence, for the same power output, PEDOT electrodes provide a material price/power that is ∼120 times lower than the Pt electrode (*SI Appendix*).

## Conclusion

In summary, we study the HET between a polymer electrode of semiconducting character and a reactant in solution. While HET at inorganic semiconductor surface strongly depends on the density of state at the Fermi level, we show that a set of semiconducting polymer electrodes with approximately the same surface density of state displays a three-orders of magnitude difference in the electron transfer rate. This reveals that the density of percolation paths for the electronic transport within the polymer electrode dictates the overall rate of electron transfer at the electrolyte–polymer electrode interface. We apply this finding to optimize the power generated by a TGC on heat-to-electricity conversion. The power can be enhanced by four orders of magnitude, demonstrating the importance of the nature of the charge transport within the conducting polymer electrodes. We believe that this finding is of key importance to optimize all of the HET for various emerging electrochemical technologies that could benefit from the unique features of conducting polymers (stability in acid medium, no surface oxide, low temperature and solution processing, porosity, abundant atomic elements). Examples of emerging technologies are fuel cells, dye-sensitized solar cells, and industrial electrochemical synthesis with low-cost conducting polymer electrodes.

## Materials and Methods

The PEDOT-PSS film was deposited on the Si substrates by spin coating the commercial aqueous dispersion Clevios PH1000 including 0.1 wt % of silane cross-linker GOPS (details can be found in *SI Appendix*). The films were about 200-nm thick as measured by atomic force microscopy (*SI Appendix*). The electrical conductivity was measured by a four-probe method, and the temperature dependence was measured in a vacuum cryogenic probe station (*SI Appendix*). Cyclic voltammetry and chronopotentiometry were performed in an aqueous solution of 10 mM $K_3Fe(CN)_6/K_4Fe(CN)_6$ in 1 M KCl as supporting electrolyte against Ag/AgCl reference electrode (details are in *SI Appendix*). Details on optical absorption and UV-photoelectron spectroscopies as well as TGC apparatus can be found in *SI Appendix*.

**ACKNOWLEDGMENTS.** X.C. thanks C. Joshua for discussion. We acknowledge the Knut and Alice Wallenberg Foundation (Tail of the Sun), the Göran Gustafsson Foundation, the Swedish Research Council, and Swedish Government Strategic Research Area in Materials Science on Functional Materials at Linköping University Faculty Grant SFO-Mat-LiU 2009-00971.

1. Chen P, McCreery RL (1996) Control of electron transfer kinetics at glassy carbon electrodes by specific surface modification. *Anal Chem* 68:3958–3965.
2. Gerischer H (1991) Electron-transfer kinetics of redox reactions at the semiconductor/electrolyte contact. A new approach. *J Phys Chem* 95:1356–1359.
3. Cline KK, McDermott MT, McCreery RL (1994) Anomalously slow electron transfer at ordered graphite electrodes: Influence of electronic factors and reactive sites. *J Phys Chem* 98:5314–5319.
4. McCreery RL (2008) Advanced carbon electrode materials for molecular electrochemistry. *Chem Rev* 108:2646–2687.
5. Peigney A, Laurent C, Flahaut E, Bacsa RR, Rousset A (2001) Specific surface area of carbon nanotubes and bundles of carbon nanotubes. *Carbon* 39:507–514.
6. Winther-Jensen B, MacFarlane DR (2011) New generation, metal-free electrocatalysts for fuel cells, solar cells and water splitting. *Energy Environ Sci* 4:2790–2798.
7. Cottis PP, et al. (2014) Metal-free oxygen reduction electrodes based on thin PEDOT films with high electrocatalytic activity. *RSC Advances* 4:9819–9824.
8. Milczarek G, Inganäs O (2012) Renewable cathode materials from biopolymer/conjugated polymer interpenetrating networks. *Science* 335:1468–1471.
9. Rahman MA, Kumar P, Park D-S, Shim Y-B (2008) Electrochemical sensors based on organic conjugated polymers. *Sensors (Basel)* 8:118–141.
10. Rivnay J, et al. (2016) Structural control of mixed ionic and electronic transport in conducting polymers. *Nat Commun* 7:11287.
11. Heinze J, Frontana-Uribe BA, Ludwigs S (2010) Electrochemistry of conducting polymers: Persistent models and new concepts. *Chem Rev* 110:4724–4771.
12. Epstein AJ, et al. (1987) Insulator to metal transition in polyaniline. *Synth Met* 18: 303–309.
13. Rudolph M, Ratcliff EL (2017) Normal and inverted regimes of charge transfer controlled by density of states at polymer electrodes. *Nat Commun* 8:1048.
14. Coskun H, et al. (2017) Biofunctionalized conductive polymers enable efficient $CO_2$ electroreduction. *Sci Adv* 3:e1700686.
15. Winther-Jensen B, Winther-Jensen O, Forsyth M, Macfarlane DR (2008) High rates of oxygen reduction over a vapor phase-polymerized PEDOT electrode. *Science* 321: 671–674.
16. Bubnova O, et al. (2014) Semi-metallic polymers. *Nat Mater* 13:190–194.
17. Chiang CK, et al. (1977) Electrical conductivity in doped polyacetylene. *Phys Rev Lett* 39:1098–1101.
18. Lee K, et al. (2006) Metallic transport in polyaniline. *Nature* 441:65–68.
19. Kang K, et al. (2016) 2D coherent charge transport in highly ordered conducting polymers doped by solid state diffusion. *Nat Mater* 15:896–902.
20. Dongmin Kang S, Jeffrey Snyder G (2016) Charge-transport model for conducting polymers. *Nat Mater* 16:252–257.
21. Ihnatsenka S, Crispin X, Zozoulenko IV (2015) Understanding hopping transport and thermoelectric properties of conducting polymers. *Phys Rev B* 92:035201.
22. Groenendaal L, Jonas F, Freitag D, Pielartzik H, Reynolds JR (2000) Poly(3,4-ethylenedioxythiophene) and its derivatives: Past, present, and future. *Adv Mater* 12:481–494.
23. Crispin X, et al. (2003) Conductivity, morphology, interfacial chemistry, and stability of poly(3,4-ethylene dioxythiophene)–Poly(styrene sulfonate): A photoelectron spectroscopy study. *J Polym Sci B Polym Phys* 41:2561–2583.
24. Xia Y, Ouyang J (2012) Significant different conductivities of the two grades of poly (3,4-ethylenedioxythiophene):poly(styrenesulfonate), Clevios P and Clevios PH1000, arising from different molecular weights. *ACS Appl Mater Interfaces* 4:4131–4140.
25. Lang U, Muller E, Naujoks N, Dual J (2009) Microscipical investigations of PEDOT. *PSS Thin Films Adv Funct Mater* 19:1215–1220.
26. Crispin X, et al. (2006) The origin of the high conductivity of poly(3,4-ethylenedioxythiophene)-poly(styrenesulfonate) (PEDOT-PSS) plastic electrodes. *Chem Mater* 18:4354–4360.
27. Ouyang J, et al. (2004) On the mechanism of conductivity enhancement in poly(3,4-ethylenedioxythiophene):poly(styrene sulfonate) film through solvent treatment. *Polymer (Guildf)* 45:8443–8450.
28. Lee I, Kim GW, Yang M, Kim TS (2016) Simultaneously enhancing the cohesion and electrical conductivity of PEDOT:PSS conductive polymer films using DMSO additives. *ACS Appl Mater Interfaces* 8:302–310.
29. Kim N, et al. (2012) Role of interchain coupling in the metallic state of conducting polymers. *Phys Rev Lett* 109:106405.
30. Nardes AM, Janssen RAJ, Kemerink M (2008) A morphological model for the solvent-enhanced conductivity of PEDOT:PSS thin films. *Adv Funct Mater* 18:865–871.
31. Håkansson A, et al. (2017) Effect of (3-glycidyloxypropyl)trimethoxysilane (GOPS) on the electrical properties of PEDOT:PSS films. *J Polym Sci B Polym Phys* 55:814–820.
32. Yu Z, Xia Y, Du D, Ouyang J (2016) PEDOT:PSS films with metallic conductivity through a treatment with common organic solutions of organic salts and their application as a transparent electrode of polymer solar cells. *ACS Appl Mater Interfaces* 8:11629–11638.
33. Wang S, et al. (2015) Experimental evidence that short-range intermolecular aggregation is sufficient for efficient charge transport in conjugated polymers. *Proc Natl Acad Sci USA* 112:10599–10604.
34. Noriega R, et al. (2013) A general relationship between disorder, aggregation and charge transport in conjugated polymers. *Nat Mater* 12:1038–1044.
35. Palumbiny CM, et al. (2015) The crystallization of PEDOT:PSS polymeric electrodes probed in situ during printing. *Adv Mater* 27:3391–3397.
36. Yan F, Parrott EPJ, Ung BSY, Pickwell-MacPherson E (2015) Solvent doping of PEDOT/PSS: Effect on terahertz optoelectronic properties and utilization in terahertz devices. *J Phys Chem C* 119:6813–6818.
37. Daum PH, Enke CG (1969) Electrochemical kinetics of the ferri-ferrocyanide couple on platinum. *Anal Chem* 41:653–656.
38. Tanimoto S, Ichimura A (2013) Discrimination of inner- and outer-sphere electrode reactions by cyclic voltammetry experiments. *J Chem Educ* 90:778–781.
39. Hu R, et al. (2010) Harvesting waste thermal energy using a carbon-nanotube-based thermo-electrochemical cell. *Nano Lett* 10:838–846.
40. Zhou H, Yamada T, Kimizuka N (2016) Supramolecular thermo-electrochemical cells: Enhanced thermoelectric performance by host-guest complexation and salt-induced crystallization. *J Am Chem Soc* 138:10502–10507.
41. Jin L, Greene GW, MacFarlane DR, Pringle JM (2016) Redox-active quasi-solid-state electrolytes for thermal energy harvesting. *ACS Energy Lett* 1:654–658.
42. Lazar MA, Al-Masri D, MacFarlane DR, Pringle JM (2016) Enhanced thermal energy harvesting performance of a cobalt redox couple in ionic liquid-solvent mixtures. *Phys Chem Chem Phys* 18:1404–1410.
43. Salazar PF, Kumar S, Cola BA (2012) Nitrogen- and boron-doped carbon nanotube electrodes in a thermo-electrochemical cell. *J Electrochem Soc* 159:B483–B488.
44. Burrows B (1976) Discharge behavior of redox thermogalvanic cells. *J Electrochem Soc* 123:154–159.
45. Ikeshoji T (1987) Thermoelectric conversion by thin-layer thermogalvanic cells with soluble redox couples. *Bull Chem Soc Jpn* 60:1505–1514.
46. Sarac H, Patrick MA, Wragg AA (1993) Physical properties of the ternary electrolyte potassium ferri-ferrocyanide in aqueous sodium hydroxide solution in the range 10-90°C. *J Appl Electrochem* 23:51–55.
47. Hirai T (1996) Charge and discharge characteristics of thermochargeable galvanic cells with an [Fe(CN)[sub 6]][sup 4–]/[Fe(CN)[sub 6]][sub 3–] redox couple. *J Electrochem Soc* 143:1305.
48. Chirea M, Borges J, Pereira CM, Silva AF (2010) Density-dependent electrochemical properties of vertically aligned gold nanorods. *J Phys Chem C* 114:9478–9488.
49. Kang TJ, et al. (2012) Electrical power from nanotube and graphene electrochemical thermal energy harvesters. *Adv Funct Mater* 22:477–489.
50. Im H, et al. (2016) High-efficiency electrochemical thermal energy harvester using carbon nanotube aerogel sheet electrodes. *Nat Commun* 7:10600.
51. Wijeratne K, Vagin M, Brooke R, Crispin X (2017) Poly(3,4-ethylenedioxythiophene)-tosylate (PEDOT-Tos) electrodes in thermogalvanic cells. *J Mater Chem A Mater* 5: 19619–19625.